Supporting Information for

Sustainable Power Sources Based on High Efficiency Thermopower Wave Devices

Sayalee G. Mahajan[1,‡], Albert Tianxiang Liu[1,‡], Anton L. Cottrill[1], Yuichiro Kunai[1], David Bender[1], Javier Castillo Jr[1], Stephen L. Gibbs[1], and Michael S. Strano[1*]

[1] 77 Massachusetts Ave, Department of Chemical Engineering, Massachusetts Institute of Technology, Cambridge, MA, USA

[‡] These authors contributed equally to this work.

[*]Corresponding author's email address: strano@MIT.edu

Table of Contents

Adiabatic Temperature Calculations

Adiabatic temperatures of NaN_3, nitrocellulose, and sucrose are calculated below. In the case of sucrose, the combustion reaction is described as shown in Equation (S1):

$$C_{12}H_{22}O_{11} + 12O_2 \rightarrow 12CO_2 + 11H_2O \quad \Delta H_c = -7.349 \times 10^5 J/mol \tag{S1}$$

where ΔH_c is the heat of combustion of the compound, in this case, sucrose. Also, ΔH_p (heat of products) is defined as in Equation (S2):

$$\Delta H_p = \int_{298}^{T^*} [12C_{p(CO_2)} + 11C_{p(H_2O)}]dT \tag{S2}$$

where T^* (K) is the adiabatic temperature, and the C_p's are the heat capacity of each product at T (K) defined as below:

$$\begin{aligned} C_{p(CO2)} &= A_{CO2} + B_{CO2} \times 10^{-3} T + C_{CO2} \times 10^{-6} T + D_{CO2} \times 10^{-9} T + E_{CO2} / (10^{-6} T^2) \\ C_{p(H2O)} &= A_{H2O} + B_{H2O} \times 10^{-3} T + C_{H2O} \times 10^{-6} T + D_{H2O} \times 10^{-9} T + E_{H2O} / (10^{-6} T^2) \end{aligned} \tag{S3}$$

The constant values of A_{CO2} through E_{H2O} are found from the database of NIST material measurement laboratory (summarized in Table 1).[1] Now, if one applies Equation (S4) to the adiabatic system, an adiabatic temperature of 1043 K can be determined for sucrose.

Table 1. Constant values for each product used in the calculations[1]

	Sucrose		Nitrocellulose			NaN_3
	$C_{p(CO2)}$	$C_{p(H2O)}$	$C_{p(CO2)}$	$C_{p(NO2)}$	$C_{p(H2O)}$	$C_{p(N2)}$
Temp Range (K)	298 - 1200	500 - 1700	1200 - 6000	1200 - 6000	1700 - 6000	500 - 2000
A	24.99735	30.092	58.16639	56.82541	41.96426	19.50583
B	55.18696	6.832514	2.720074	0.738053	8.622053	19.88705
C	-33.69137	6.793435	-0.492289	-0.144721	-1.49978	-8.598535
D	7.948387	-2.53448	0.038844	0.009777	0.098119	1.369784
E	-0.136638	0.082139	-6.447293	-5.459911	-11.15764	0.527601

$$\Delta H_p + \Delta H_c = 0 \tag{S4}$$

Adiabatic temperatures for nitrocellulose and NaN_3 were also estimated to be 2427 K and 760 K, respectively. The reactions considered are described below:

$$\left[C_6H_7O_2(ONO_2)_3\right] + \frac{21}{4}O_2 \rightarrow 6\,CO_2 + 3\,NO_2 + \frac{7}{2}H_2O \quad H_c = -1.247 \times 10^6 J/mol \tag{S5}$$

$$N_3^- \rightarrow \frac{3}{2}N_2 + e^- \qquad H_c = -2.081\times10^4 J/mol \tag{S6}$$

In the case of NaN_3, the predominant reaction is the azide decomposition, as reported by Abrahamson *et al.*, with the azide ion decomposing into gaseous nitrogen and the sodium moiety remaining on the SWNT.[2] As a result, only the generation of nitrogen is taken into consideration. This decomposition mechanism has been well-studied and documented.[3,4]

Raman Spectroscopy Measurement Details

The G peak of SWNT fiber samples was measured by using a confocal Raman spectrometer (Horiba Jobin-Yvon LabRAM Raman Microscope), as shown in Figure S1a. Excitation was performed using a 532 nm solid-state diode pumped laser (Kaiser Optical Systems, Inc., Invictus 532 nm VIS Laser). The measurement was performed 25 times on each sample, with gradual changing of the position of the sample. In the analysis, the error bars denote a 95 % confidence interval.

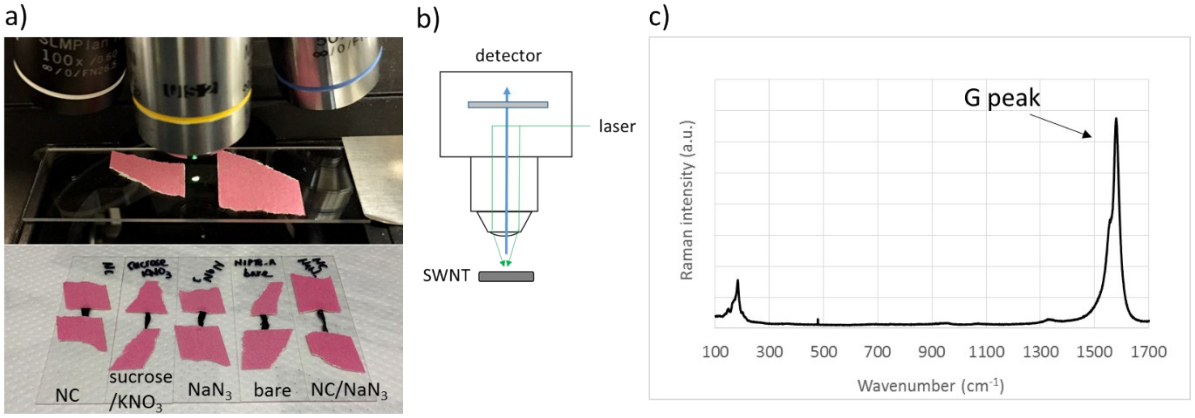

Figure S1. (a) Pictures of samples and the confocal Raman spectrometer. (b) Schematic illustration of the Raman spectrometer, green line is laser incident light and blue line is the Raman scattering. c) Typical Raman spectrum for a bare SWNT fiber, which has a G peak located around 1577 cm^{-1}.

Fermi Energy Estimations

Fermi energies of doped SWNTs were estimated from the correlation reported by Farhat *et al.*[5] They reported that the G band shift of metallic SWNTs is sensitive to Fermi level changes, while that of semi-conductive SWNTs is not. Since our current samples are a mixture of metallic and semi-conductive SWNT, the Fermi level change of metallic SWNTs is responsible for the Raman G peak shift. Furthermore, because the Fermi level of the doped semi-conductive SWNTs remains the same, the Fermi level of the SWNT ensembles can be estimated from the G peak shift of the pure metallic SWNTs.

Both p-doping and n-doping show up-shift of the G peak, so basically, two values of the Fermi level, from p-doping or n-doping, can be estimated from the data of Farhat *et al*. Therefore, -0.23 eV (p-doping) and +0.40 eV (n-doping) are obtained for NaN_3 doped SWNT from a 1579cm^{-1} G peak. In the case of Bare SWNTs, the G peak position is measured to be 1577 cm^{-1} and also they are known to be p-doped by oxygen, so a Fermi level of -0.21 eV is only assigned. Nitrocellulose/NaN_3 doped SWNT has a 1584 cm^{-1} G peak. In this case, it should be p-doping, because the G peak of n-doping is almost saturated around 1580 cm^{-1} and never reached up to 1584 cm^{-1}.

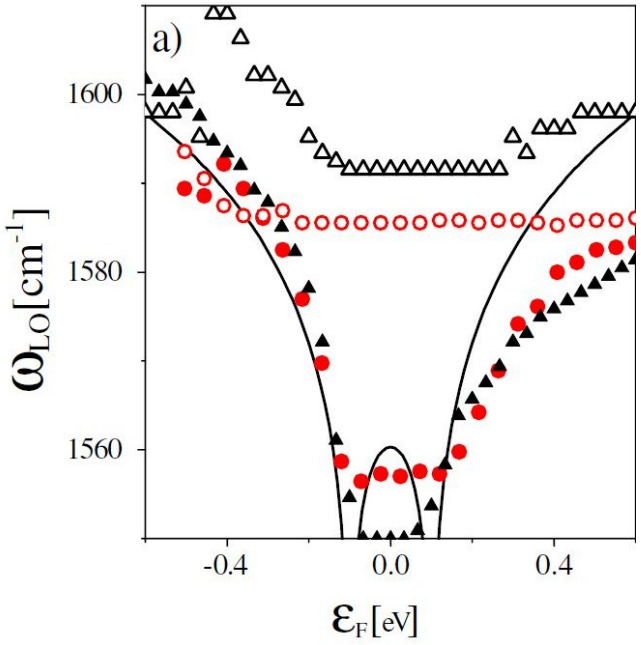

Figure S2. Correlation obtained from the report of Farhat *et al*., which plots the G peak shift as a function of the Fermi level. Closed red circle data shows the behavior of metallic SWNTs, which we used for the Fermi level estimation.[5]

Generalized TPW Device Fueling and Manufacturing Procedure

Several fuels were added onto SWNT fibers or yarns in this report. The basic procedure is given below with a typical example of NaN_3. Initially, NaN_3 in water solution was prepared (30 g NaN_3 per L of water). The concentration can be changed depending on the target fuel ratio. Fueling was done using a dipping method, where the NaN_3 solution was poured around the bare SWNT yarn in a petri dish, then dried for approximately 6 hours in ambient conditions. The bare SWNT yarns (Nanocomp Technologies Inc., Carbon Nanotube Yarn) and the bare SWNT fibers (KH Chemicals, KH Single-walled Carbon Nanotube) were used as purchased. This fueling procedure was repeated until the fuel ratio (fuel mass: SWNT mass) reached the

target ratio. A schematic of this procedure and a picture of NaN_3 doped SWNT yarns are shown in Figure S3a and S3b, respectively. With the SWNT yarn properly fueled, we proceed to make the TPW device, which involves preparing a structural support and two copper electrodes. The SWNT conduit is taped onto the copper electrode using copper tape and then covered with silver paste to ensure good electronic contact (Figure S3c and S3d).

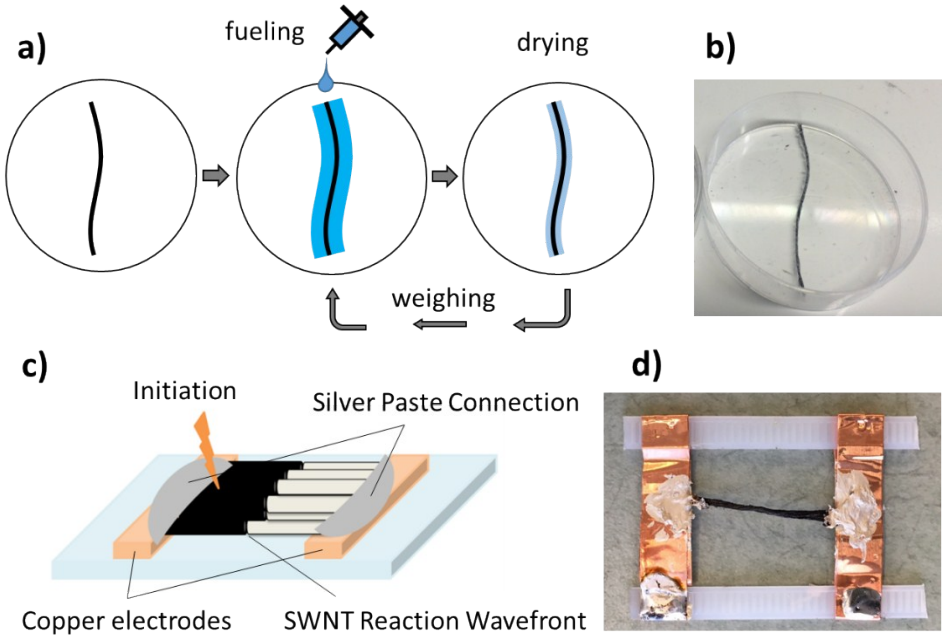

Figure S3. (a) A schematic for the procedure of fueling. The NaN_3 in water solution was poured around SWNT yarn, then dried for approximately 6 hours in ambient conditions. (b) A picture of the NaN_3 doped SWNT yarn. (c) A schematic and (d) a picture of a typical TPW device, with a SWNT yarn, copper electrodes, silver paste and support shown.

Using Residual Energy Harvesting Devices to Augment TPW Efficiency

We prepared a device for illuminating an LED by connecting 4 (4.0 cm x 4.0 cm) commercial Bi_2Te_3 thermoelectric harvesters and a thermopower wave device in series. First, a box with 4 windows for fixing the thermoelectric harvesters was made, as shown Figure S4a through S4d. Reflective aluminum foil was used inside the box in order to focus the heat energy onto the thermoelectrics. The thermopower wave device was made as shown in Figure S4e. Three NaN_3 doped SWNT yarns were connected in parallel via copper tape and placed inside the box. Finally, thermoelectric harvesters and the TPW device were connected in series, as shown in Figure S4f.

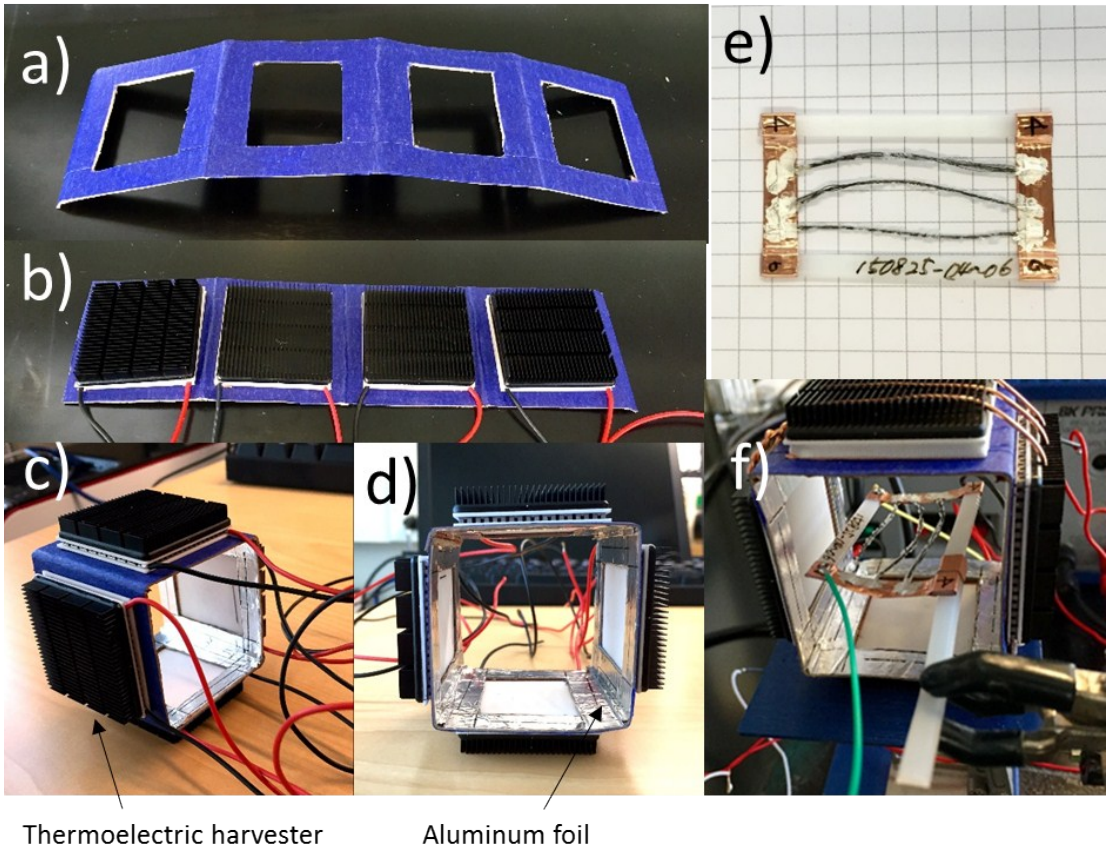

Figure S4. (a-d) Pictures of preparation of the thermoelectric harvesters preparation. Aluminum foil was pasted inside the box as a reflector. (e) Thermopower wave devices of three NaN_3 doped SWNT yarns in parallel. f) Device with the thermoelectric harvesters and the TPW device inside the box, which are connected in series.

Illuminating an LED for 20 s

An LED and the device shown in Figure S4 were connected through a voltage step-up converter (Linear Technology Co., Ltd, LTC3109EUF) in order to obtain the 1.5 V necessary to illuminate the red LED. The successive ignitions of three NaN_3-SWNT TPW devices and the simultaneous thermoelectric harvesting created a voltage, which was amplified by the voltage step-up converter and harnessed to power the LED. A series of photographs illustrating the illumination of the LED is provided in Figure S5a through S5h. The LED illuminated at 1.5 V and maintained its intensity for over a period of 20 seconds.

Figure S5. (a-h) Successive pictures demonstrating the illumination of an LED using TPW devices with external energy harvesting. The insets for each subfigure show an enlarged photograph of the LED. The multi-meter displays an output voltage of the step-up converter.

Seebeck Coefficient Measurements of SWNT Yarns

The Seebeck coefficient of SWNT yarns was measured by the following method. A 6 cm SWNT yarn was used in order to create a distinguishable temperature bias. One end of the SWNT yarn was heated, while the other end was cooled in ambient air, as shown in Figure S6a and S6b. The temperature of both ends were measured by thermocouples. Both ends of the SWNT yarn were also connected to a multi-meter for voltage measurements. In this method, the Seebeck coefficient was estimated to be 28.2 (μV/K) using Equation (S7):

$$S = \frac{V}{\Delta T} (\mu V/K) \tag{S7}$$

where S (μV/K) is the Seebeck coefficient, V (μV) is the open circuit voltage and ΔT (K) is temperature difference across the SWNT yarn.

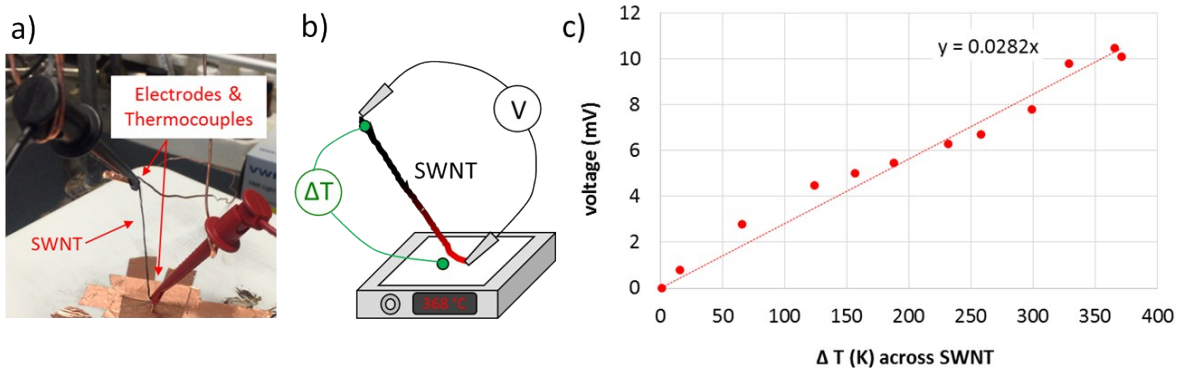

Figure S6. (a) Picture and (b) schematic illustration of the measurement setup for the Seebeck coefficient. (c) Relationship between the open circuit voltage and ΔT across the SWNT yarn.

Modeling Details for the Wave Propagation with Thermal and Electronic Transport

1. Motivating a Simplified Heat and Mass Balance Based Reaction Model to Analyze the Voltage Output from Thermopower Wave Devices

Thermopower wave devices convert chemical energy into electrical energy via self-propagating reaction waves. A layer of fuel coated atop a thermal conduit is used to launch this self-propagating reaction wave that is initiated from one end of the device. For any chemical reaction carried out in an adiabatic system, which disallows transfer of heat and mass of its contents with the surroundings, the difference between the temperature reached by the products of the reaction once the reaction is complete and the temperature of the system at the start of the reaction is known as the adiabatic reaction temperature (rise) for that chemical reaction. Theoretical and numerical analysis shows that, for a steady state thermopower wave type of self-propagating reaction wave launched in an adiabatic system, the temperature behind the reaction wave front should be the adiabatic reaction temperature of the chemical reaction being carried out (plus the ambient or initial temperature).[6] At the same time, the unreacted region of the fuel-thermal conduit will be at the ambient temperature or the initial temperature of the device. Thus, while the reaction is propagating, there exists a temperature difference equivalent to the adiabatic reaction temperature rise across the ends of the thermopower wave system. Moreover, the region of the thermal conduit that is coated with the fuel is doped due to the adsorbed fuel molecules.[2] As the reaction proceeds and the fuel molecules desorb, a chemical potential difference is established across the ends of the device. Thus as the self-propagating reaction wave proceeds along the length of the thermopower wave device, there is a temperature difference and a chemical potential difference created across the ends of the device. Both of these lead to the generation of a voltage output that can be harvested across the ends of the thermopower wave device as electrical output.

Thermopower wave devices can be studied as constant voltage sources giving rise to an open circuit voltage difference (ΔV_{OC}). When connected to an external electrical load, we can obtain useable output voltage (ΔV_{out}) and current flow through the load. In an ideal adiabatic system, during the entire duration of the reaction wave propagation, the magnitude of the temperature difference and the chemical potential difference should remain constant for a chosen pair of uniformly-coated fuel and thermal conduit. Thus, if we can estimate the magnitude of the thermal difference and the chemical potential difference for a system with a known Seebeck coefficient S, we can calculate the expected open circuit voltage (ΔV_{OC}). Using the values of the internal resistance of the thermopower wave device (R_{int}) and the resistance of the load attached (R_{ext}), we can compute the expected output voltage (ΔV_{out}).

In practice, however, for a thermopower wave device, factors such as conductive heat losses to the copper electrodes and radiative/convective heat losses to the surroundings lead to the actual temperature difference not only being lower than that expected under adiabatic conditions but also time variant. Similarly, depending on the electrical properties of the thermal conduit and the fuel-coated thermal conduit, the internal resistance of the device (R_{int}) changes as the reaction proceeds. As the reaction wave proceeds, the fraction of the device length is heated changes. This can affect the net internal resistance of the device, especially in the case of thermal conduits such as carbon nanotubes which exhibit temperature-dependent resistivity.[7] Ideally, the chemical potential difference should also be dependent on only the fuel-thermal conduit pair and should remain constant as long as there is uniform reaction wave propagation. However, factors such as non-uniform coating of the fuel layer and a lack of enough fuel to coat the entire conduit surface area lead to a lowered level of doping, which results in a variable chemical potential difference across samples. Also, this chemical potential difference ceases to exist as soon as the reaction has completely propagated or has stopped after partial propagation. In cases where the reaction propagation ceases and the reaction wave front reaches the opposite end of the thermal conduit, the temperature gradient does not necessarily drop to zero, as the 'other' side of the thermal conduit, where the reaction wave was launched, cools during the time of reaction propagation. Thus, depending on the internal heat transfer properties of the system and the rate at which it loses heat to the surroundings, there is a possibility of reversal of the temperature difference, leading to an opposite polarity voltage output contribution due to the thermoelectric effect. Interplay of factors such as time-dependence of the temperature difference and the chemical potential difference and practical conditions for device operation (e.g., non-adiabatic system and device-to-device differences in the experiments) can possibly explain the variety of voltage outputs (*e.g.,* double polarity voltage output, single polarity voltage output*)* obtained from the thermopower wave devices.

To gain more understanding about voltage output from thermopower wave devices, a theoretical model for analyzing self-propagating reaction waves was developed. This model, based on heat and mass transfer balances and the theory of excess thermopower, computes the TPW voltage output for different scenarios of reaction and heat propagation. With this model, via known or calculated thermal and electrical properties of the system, we can calculate the expected electrical output for a chosen fuel-thermal conduit thermopower wave system. Using this model, one can reverse calculate the fuel and system properties needed in order to obtain a specific voltage output profile, as may be needed for any specific power application. We demonstrate using this model for fitting the experimental data from SWNT-nitrocellulose (and sodium azide) TPW devices. We analyze the experimentally obtained voltage output profiles by fitting for various parameters in the model and learn more about the heat transfer and electrical properties of our system.

2. Method of Lines Applied to Solve a 1D Time Variant Heat and Mass Transfer System

To predict the voltage output from a thermopower wave device, we need to calculate the voltage contribution due to the thermoelectric effect (*i.e.,* the temperature difference) and the voltage contribution due to the excess thermopower (*i.e.,* the chemical potential difference). To calculate the temperature difference across the end of the system as a function of time, we solve a system of heat and mass transfer equations that simulates thermopower wave propagation. Using the magnitude of the temperature difference, with the value of the Seebeck coefficient S of the system, we calculate the thermoelectric contribution of the voltage output. For a known or fitted value of the chemical potential difference (which we assume stays constant and active during the reaction wave propagation), we then estimate the value of the voltage contribution due to excess thermopower. Thus, using the information about the temperature difference and the chemical potential difference, along with other physical properties of the system, the final expected voltage output of the system could be calculated. When fitting the experimental data for system property parameters, this model output voltage profile (generated using some initial guess values for the fitted parameter values) is compared with the experimentally obtained output voltage profile. With the aim of minimizing this difference, we fit values to the parameters involved (e.g., the Seebeck coefficient of the system S, the magnitude of the chemical potential difference $\Delta\mu$, and the conductive losses via copper electrodes, *etc.*) until a satisfactory fit is obtained. Thus, using this model, we can extract parameter values representative of our experimental system. These can then be used with the model to then predict other future voltage output profiles that can be obtained experimentally. Analyzing these parameter values for a variety of voltage output data can help in studying device-to-device variation and guide us toward the key characteristics of higher efficiency devices.

As shown previously,[8] a 1D self-propagating reaction wave can be analyzed by studying the corresponding heat and mass transfer equations for a system of continuous fuel layer undergoing reaction in a one-dimensional system. This continuous layer of a fuel is provided with input heat to initiate the reaction wave. Internal heat transfer properties of the system control the heat propagation that leads to the sustenance of the reaction wave. The external heat transfer properties of the system allow us to model the heat lost by the reaction system to the surroundings. In this model, we account for conductive heat loss via the ends of the fuel layer, as well as convective and radiative losses from the TPW device.

The corresponding set of heat and mass balance equations being studied is presented below. In equations (S8) and (S9), T denotes the temperature, Y denotes the fuel concentration, t denotes the time and x denotes the space coordinate. The subscripts are used to denote the type of the property and/or the material it is attributed to. We assume that the reaction system starts at the ambient temperature, T_{amb}. The system's temperature profile changes as heat is released from the reaction wave. Heat is generated in the system due to the propagating reaction wave, which releases heat via -ΔH, the heat of reaction. Fuel reaction is modeled by assuming first order reaction. E_a denotes the activation energy of the reaction and k_0 denotes the Arrhenius pre-exponential factor. Since the thermal mass of carbon nanotubes dominates that of the fuel (which often gets converted to mainly gaseous products post-reaction), the energy balance equation considers the thermal mass of the carbon nanotubes to be representative of the system. We make this assumption since we know that the thermal transport is dominated by transport though the carbon nanotubes rather than the layer of the fuel surrounding the cluster of carbon nanotubes. Previous work analyzing a more detailed model consisting of separate energy balances for the fuel and thermal conduit showed that for practical systems consisting of carbon nanotubes based thermal conduits, there is a fast thermal equilibrium between the thermal conduit and the fuel layer, leading to almost equal temperature profiles.[8] Thus the thermal mass of the system can be calculated using the density of carbon nanotubes ρ_{CNT} and the specific heat capacity of carbon nanotubes $C_{p,CNT}$.

$$\rho_{CNT} C_{p,CNT} \frac{\partial T}{\partial t} = k_{CNT} \frac{\partial^2 T}{\partial x^2} - \Delta H k_o Y e^{-\frac{E_a}{RT}} - \varepsilon \sigma_B \left(\frac{A_{Surface}}{V} \right) \left(T^4 - T_{amb}^4 \right) - h_{conv} \left(\frac{A_{Surface}}{V} \right) \left(T - T_{amb} \right) \quad \text{(S8)}$$

$$\frac{\partial Y}{\partial t} = -\left(k_o Y \right) e^{-\frac{E_a}{RT}} \quad \text{(S9)}$$

The energy balance for the continuous fuel system is as shown in equation (S8). During practical experimental conditions, while the reaction wave is propagating across the length of the device, it loses heat through multiple modes such as conductive heat losses through the copper electrodes, convective heat losses to the surrounding air, convective heat losses via the

gaseous products leaving the system, and radiative losses. The two right-most terms of Equation (S8) account for the radiative and convective losses from the fuel system to the surroundings. Here, ($A_{surface}/V$) denotes the device's surface area per volume that is active when losing heat to the surroundings and h_{conv} is the convective heat transfer coefficient. The mass balance equation which assumes the 1st order Arrhenius form of reaction for the fuel is as shown in Equation (S9).

For the ease of solving these coupled heat and mass balance equations, we non-dimensionalize the variables of temperature, fuel concentration, time, and space coordinate to define non-dimensional variables u, y, τ, and ξ, respectively. Non-dimensional forms of the heat and mass balance equations are shown in Equations (S14) and (S15).

$$u = T\left(\frac{R}{E_a}\right) \tag{S10}$$

$$y = Y\left(\frac{1}{\rho_{CNT}}\right) \tag{S11}$$

$$\tau = t\left(\frac{(-H)k_0 R}{C_{p,CNT} E_a}\right) \tag{S12}$$

$$\xi = x\sqrt{\left(\frac{\rho_{CNT} C_{p,CNT}}{k_{CNT}}\right)\left(\frac{(-\Delta H)k_0 R}{C_{p,CNT} E_a}\right)} \tag{S13}$$

$$\frac{\partial u}{\partial \tau} = \frac{\partial^2 u}{\partial \xi^2} + y e^{-\frac{1}{u}} - w_{rad}(u^4 - u_{amb}^4) - w_{conv}(u - u_{amb}) \tag{S14}$$

$$\frac{dy}{d\tau} = -\beta y e^{-\frac{1}{u}} \tag{S15}$$

Here, w_{rad} corresponds to the non-dimensional net radiative heat transfer coefficient. For a known ($A_{surface}/V$), we can estimate w_{rad} for a chosen system. Similarly, w_{conv} corresponds to the non-dimensional net convective heat transfer coefficient. Non-dimensionalization of variables also gives rise to the important non-dimensional factor of β, the inverse non-dimensional adiabatic temperature rise of the fuel. Thus [($1/\beta$) + u_{amb}] gives the maximum non-dimensional temperature that can be reached by the system.

$$\beta = \frac{C_{p,CNT} E_a}{(-\Delta H) R} \tag{S16}$$

To obtain the time-dependent temperature difference along the ends of the device, we need to solve the above set of partial differential equations. To simplify solving this set of partial differential equations, we use the technique of Method of Lines. This method involves discretization along one of the two independent variables (τ and ξ) to convert the set of partial differential equations to a set of ordinary differential equations. In this case, as shown in Equation (S17), we discretize along the distance coordinate by using the central difference form for simplifying the second order derivative term in Equation (S14). When applying the method of lines, the entire domain along the direction ξ is divided into grid points at a distance of $\Delta\xi$. Assuming we divide the domain in ($n+1$) equal regions, $\Delta\xi$ can be calculated by dividing the non-dimensional sample length ξ_{spl} into ($n+1$) parts. The 1st and the last point on this new grid, denoted by subscript *0* and ($n+1$), act as interfaces between the surroundings at ambient temperature u_{amb}.

For a general point *i* within the reaction domain, the second order derivative with respect to the space coordinate can be simplified using Equation (S17). Substituting for discretization along the space coordinate, the partial differential heat transfer equation (S14) is converted to a system of ordinary differential equations, as shown in Equation (S18). This equation applies to each grid point i = (*1* to n) along the reaction domain.

$$\left.\frac{d^2u}{d\xi^2}\right|_i = \frac{u_{i+1} - 2u_i + u_{i-1}}{\Delta\xi^2} \tag{S17}$$

$$\frac{du_i}{d\tau} = \frac{u_{i+1} - 2u_i + u_{i-1}}{\Delta\xi^2} + y_i e^{-\frac{1}{u_i}} - w_{rad}(u_i^4 - u_{amb}^4) - w_{conv}(u_i - u_{amb}) \tag{S18}$$

$$\frac{dy_i}{d\tau} = -\beta y_i e^{-\frac{1}{u_i}} \tag{S19}$$

In this model, we account for the external heat transfer losses via conduction through the ends of the device to the copper tape electrodes. The copper tape electrodes are assumed to always be at the non-dimensional temperature u_{amb}, and the conductive heat transfer coefficient k_e=k_{Cu} is assumed to act over an external heat transfer length scale L_e. These values, along with the thermal conductivity of the thermal conduit, give rise to the thermal flux boundary conditions provided in Equation S20 and S21. We ignore the variation in the cross-sectional area across

at which the heat transfer occurs (i.e., $A_i=A_e=A_{CNT}$.) In defining the conductive heat loss through the system, we define two more heat transfer coefficients acting in the system: the internal heat transfer coefficient $g_i=k_{CNT}/\Delta\xi$ and the external heat transfer coefficient $g_e=k_e/L_e$.

$$\frac{k_e}{L_e}(u_{amb}-u_0)=\frac{k_{CNT}}{\Delta\xi}(u_0-u_1)$$
$$\therefore u_0=\frac{\left(\frac{k_e}{L_e}u_{amb}+\frac{k_{CNT}}{\Delta\xi}u_1\right)}{\left(\frac{k_e}{L_e}+\frac{k_{CNT}}{\Delta\xi}\right)} \tag{S20}$$

$$\frac{k_{CNT}}{\Delta\xi}(u_n-u_{n+1})=\frac{k_e}{L_e}(u_{n+1}-u_{amb})$$
$$\therefore u_{n+1}=\frac{\left(\frac{k_e}{L_e}u_{amb}+\frac{k_{CNT}}{\Delta\xi}u_n\right)}{\left(\frac{k_e}{L_e}+\frac{k_{CNT}}{\Delta\xi}\right)} \tag{S21}$$

These boundary conditions can be used to simplify the heat transfer equations at the grid points *1* and *n*. Thus, after employing the technique of method of lines and modeling the heat loss through the ends of system as conductive losses, the updated set of equations governing the reaction domain between interfaces is given below in Equations (S22-S25).

$$\frac{du_1}{d\tau}=\frac{u_2}{\Delta\xi^2}+\frac{\left(-2\frac{k_e}{L_e}-\frac{k_{CNT}}{\Delta\xi}\right)}{\left(\frac{k_e}{L_e}+\frac{k_{CNT}}{\Delta\xi}\right)}\frac{u_1}{\Delta\xi^2}+\frac{\left(\frac{k_e}{L_e}\right)}{\left(\frac{k_e}{L_e}+\frac{k_{CNT}}{\Delta\xi}\right)}\frac{u_{amb}}{\Delta\xi^2}+y_1e^{-\frac{1}{u_1}} \tag{S22}$$

$$\frac{du_i}{d\tau}=\frac{u_{i+1}-2u_i+u_{i-1}}{\Delta\xi^2}+y_ie^{-\frac{1}{u_i}}-w_{rad}(u_i^4-u_{amb}^4)-w_{conv}(u_i-u_{amb}) \tag{S23}$$

$$\frac{du_n}{d\tau}=\frac{\left(-2\frac{k_e}{L_e}-\frac{k_{CNT}}{\Delta\xi}\right)}{\left(\frac{k_e}{L_e}+\frac{k_{CNT}}{\Delta\xi}\right)}\frac{u_n}{\Delta\xi^2}+\frac{\left(\frac{k_e}{L_e}\right)}{\left(\frac{k_e}{L_e}+\frac{k_{CNT}}{\Delta\xi}\right)}\frac{u_{amb}}{\Delta\xi^2}+\frac{u_{n-1}}{\Delta\xi^2}+y_ne^{-\frac{1}{u_n}} \tag{S24}$$

$$\frac{dy_i}{d\tau} = -\beta y_i e^{-\frac{1}{u_i}} \tag{S25}$$

This coupled set of Equations (S22-S25) when solved with appropriate initiation condition allows us to fully characterize the temperature and the fuel concentration profile of the thermopower wave device. The input heat needed to start the reaction can be simulated by setting the temperature of the grid point 1 at zero time or start of the reaction to a threshold value for the fuel reaction to be activated. From the previous work in analyzing self-propagating reaction waves in one dimension, the minimum non-dimensional temperature needed to initiate the fuel reaction was found to be $g=g_0e^{0.37\beta}=0.16e^{0.37\beta}$.[8]

Since experimental work has shown that nitrocellulose begins showing reduction in weight due to reaction starting at about 175 °C.[9] Partial propagation of the reaction wave can be modeled by setting the input fuel concentration of *nofuel* number of grid points (at the end of the system) to zero. When fitting the experimental data, the value of *nofuel* is chosen to agree with the fraction of partial wave propagation. Thus, knowing the value of the percent conversion or percent propagation along the length of the sample, *nofuel* can be calculated for the chosen value of n.

Using this temperature profile obtained by solving Equations (S22-S25) and with Equations (S20) and (S21), we can calculate the temperature difference established across the ends of the system by calculating (u_{n+1}-u_0). Using the value of the energy of activation E_a, we can convert this non-dimensional temperature difference into a dimensional temperature difference (T_{n+1}-T_0). For known S, the Seebeck coefficient of the carbon nanotube – fuel system, we can calculate $\Delta V_{TE}(t)$, the expected thermoelectric voltage output from the system. In practice, the Seebeck coefficient of the system is a temperature-dependent property, and, thus for a realistic thermopower wave system, should vary with time. However, for the ease of modeling, we assume it to be a fixed quantity that does not vary with time, but varies from device to device.

$$\Delta V_{TE}(t) = S\left(T_{n+1}(t) - T_0(t)\right) \tag{S26}$$

The theory of excess thermopower predicts that the voltage output from the thermopower wave devices also has a contribution from $\Delta\mu$, the chemical potential difference that is established across the ends of the system. This gradient drops to zero once the reaction wave has fully propagated and all the fuel coated atop the thermal conduit has reacted. In case of partial reaction wave propagation, when the reaction wave propagation halts, there still exist two regions, fuel-coated and bare thermal conduit. However, in such a situation, we hypothesize

that the charge carriers internally diffuse towards equilibration within the thermal conduit layer (rather than flowing through the external electrical circuit), thus not contributing to a measurable voltage output. Hence, even in case of partial reaction propagation, the excess thermopower wave voltage contribution has been assumed to stop as soon as the reaction wave propagation halts. Knowing $\Delta\mu$, we can calculate ΔV_{excess}, the excess thermopower contribution to the net voltage output across the thermopower wave device.

$$\Delta V_{Excess}(t) = -\frac{1}{e}(\Delta\mu(t)) \tag{S27}$$

We assume the ideal thermopower wave device preparation, where the fuel dopes the thermal conduit uniformly, and therefore, the chemical potential gradient is only a function of the presence of a moving reaction wavefront. Changes in values of $\Delta\mu$ as obtained while fitting experimental voltage output profiles from different samples using the same fuel-thermal conduit combination could be insightful in trying to understand the types of voltage outputs we observe and point to inconsistencies in sample preparation.

ΔV_{TPW} or ΔV_{OC}, the net (open circuit) voltage output from the thermopower wave device is given by both the thermoelectric voltage output and the excess thermopower output.

$$\Delta V_{TPW} = \Delta V_{OC} = \Delta V_{TE} + \Delta V_{Excess} \tag{S28}$$

The time variance in the presence of the chemical potential gradient is accounted for by making its contribution dependent on the presence of the reaction wave. This is done by keeping the $\Delta V_{\mathrm{excess}}$ contribution 'on' as long as the reaction wave propagates. Turning 'off' the $\Delta V_{\mathrm{excess}}$ is triggered by the fuel concentration of the last filled reactor falling below 10^{-2}.

$$\begin{aligned} &\Delta V_{TPW} = \Delta V_{TE} + \Delta V_{Excess} \\ &\therefore \Delta V_{TPW} = S(T_{n+1} - T_0) - \frac{1}{e}(\Delta\mu)(y_{lastfilled} - y_1) \end{aligned} \tag{S29}$$

Equation (S29) gives the voltage output equivalent of an open circuit voltage output for a voltage source. For more accurate power and energy output calculations, the experimental data is collected for the voltage output across an external resistance R_{ext}. Hence, when predicting the experimental voltage output, we need to calculate the (closed circuit). R_{int} denotes the internal resistance of the thermopower wave device. The resistance is a function of temperature and should change as the reaction propagates along the length of the device. Also, the presence of the fuel layer on the carbon nanotubes leads to changes in the resistance, and thus, the device internal resistance is expected to change as the fuel reacts. However, to simplify the model, we

assume the resistance to be a time (and temperature) invariant property. Experimentally, R_{int} is the average of the TPW device resistance, measured before and after the reaction propagation.

$$\begin{aligned}
&\Delta V_{out} = \Delta V_{OC} - IR_{\text{int}} \\
&\therefore \Delta V_{out} = S\left(T_{n+1} - T_0\right) - \frac{1}{e}(\Delta\mu)\left(y_{lastfilled} - y_1\right) - IR_{\text{int}} \\
&\therefore \Delta V_{out} = S\left(T_{n+1} - T_0\right) - \frac{1}{e}(\Delta\mu)\left(y_{lastfilled} - y_1\right) - \left(\frac{\Delta V_{out}}{R_{ext}}\right)R_{\text{int}} \\
&\therefore \Delta V_{out} = \frac{S\left(T_{n+1} - T_0\right) - \frac{1}{e}(\Delta\mu)\left(y_{lastfilled} - y_1\right)}{1 + \frac{R_{\text{int}}}{R_{ext}}}
\end{aligned} \tag{S30}$$

Equation (S30) predicts the output voltage expected from a TPW device having an internal resistance R_{int}, Seebeck coefficient S, fuel-dependent chemical potential gradient $\Delta\mu$, and external load resistance R_{ext}. Thus, summarizing the steps involved in practicing this model in order to evaluate the output voltage profile, we need values for the following parameters: ρ_{CNT}, $C_{p,CNT}$, k_{CNT}, k_e/L_e, β, k_0, E_a, S, $\Delta\mu$, R_{int}, R_{ext}, sample length L_{spl}, $\Delta\xi$ or n, *nofuel,* ($A_{surface}/V$) and h_{conv}. We note the literature values for various properties for nitrocellulose (NC) and carbon nanotubes (CNT) as shown in Table 2 and Table 3.

Table 2: Properties of Nitrocellulose (NC)

Parameter	Value	Source
E_a	32.6 (kcal mol^{-1})=136.4 (kJ mol^{-1})	Chen & Brill[9]
(-ΔH)	4200 (J gm^{-1})	Kim et al.[10]
k_0	$\log_{10}(k_0) = 16.4$ [s^{-1}] Or $k_0=2.512*10^{16}$ s^{-1}	Chen & Brill[9]

Table 3: Properties of Carbon Nanotubes (CNT)

Parameter	Value	CNT Specifications	Source
$C_{p,CNT}$	0.65 (J gm^{-1} K^{-1})	300 K for SWNT ropes samples	Hone et al.[11]
$k_{i,CNT}$	36 (J s^{-1} m^{-1} K^{-1})	Dense-packed SWNT mat	Hone et al.[12]

δ_{CNT} (Resistivity)	10^{-6} (Ω m)	Crystalline metallic SWNT	Thess et al.[13]
ρ_{CNT}	$1.4x10^{6}$ (g m^{-3})	Metallic SWNT ropes	Collins et al.[14]

3. Procedure for Predicting and Fitting Experimental Data

With known values for the thermopower wave device system properties, we can use the model to predict the form of the output voltage profile. Alternatively, we can use the model with the experimental voltage output to fit for various parameters for our experimental system. For simplifying the fitting process for SWNT-nitrocellulose based TPW devices, we calculate β using the literature values for specific heat of carbon nanotubes and heat of reaction for nitrocellulose. The value was found to be 2.54. However, because nitrocellulose is a polymer with a poorly understood reaction mechanism, we fit for the reaction parameters k_0 and E_a. For calculating the dimensionless length, we use literature values for the thermal conductivity of carbon nanotubes ($k_{i,CNT}$) and the density of carbon nanotubes (ρ_{CNT}). The value of R_{ext} was chosen as 47 Ω. The initial temperature profile was assumed to be 298 K. Similarly, the initial, nondimensional fuel concentration profile was set to 1 for fueled grid points and 0 for *nofuel* grid points. For these parameter fittings, the value of n was chosen to be 100 on the basis of previous practice runs where n was also one of the system parameters that was optimized for to obtain the best possible prediction of the system voltage output. A list of all the input parameters is shown in Table 4.

Table 4: TPW Model Parameters: Inputs

Parameter	***Parameter Description***	***Input Form***
$\beta = \frac{C_{p,CNT} E_a}{(-\Delta H) R}$	Inverse of the non-dimensional adiabatic temperature rise for the chosen fuel	Fixed and calculated input
$C_{p,CNT}$=0.65 (J gm^{-1} K^{-1})	Specific heat capacity of carbon nanotubes	Literature input used to calculate β
$k_{i,CNT}$ = 36 (J s^{-1} m^{-1} K^{-1})	Thermal conductivity of carbon nanotubes	Literature input to non-dimensionalize
ρ_{CNT} = $1.4x10^{6}$ (g m^{-3})	Density of carbon nanotubes	Literature input to non-dimensionalize
R_{int}	Average internal resistance of the thermopower wave device (Ω)	Experimental input

R_{ext} = 47 Ω	External resistance used to measure the TPW output voltage	Experimental input
$g=g_0e^{(0.37\beta)}$	Initiation heat pulse (non-dimensional temperature) provided to the 1st grid point	
y_0	Fuel quantity in each reactor (either 1 or 0)	User Input to decide fuel content in filled and *nofuel* reactors
u_{amb}	Non-dimensional ambient temperature	Input assuming 298 K
n=100	Number of length scale units in the system	Fixed
nofuel	Number of un-fueled grid points in the system	Experimental input from % propagation or % conversion

Using the inputs from Table 4, we fit for the remaining parameters. Table 5 provides a list of the parameters being optimized for and the interpretation from each parameter fitted.

Table 5: TPW Output Voltage Model Parameters: Outputs

Parameter	***Parameter Description***
$g_e=k_e/L_e$	External heat transfer coefficient for the transfer between the reaction system and the copper electrodes (conductive transfer)
S	Seebeck Coefficient of the TPW system (μV/K)
Δμ	Chemical Potential Gradient (Coulombs-Volts)
k_0	Arrhenius pre-exponential factor (s^{-1}) such that $\tau_{fac}=\left(\frac{C_{p,CNT}E_a}{(-H)R}\frac{1}{k_0}\right)=\frac{\beta}{k_0}$ Used to calculate non-dimensional time step equivalent of experimental voltage data time steps of $\Delta t_{\exp}=0.0005$ s
E_a	Activation Energy for the fuel reaction (J mol^{-1})
$(A_{surface}/V)$	Exposed area per unit volume, which contributes to convective and radiative heat loss along the length of the device, calculated using the fitted w_{rad}.

h_{conv}	Calculated using w_{conv}, it represents the convective heat transfer coefficient for the device.

We start the fitting procedure by using the input and guess values for all the parameters involved in the model (from Table 4 and Table 5). We then solve the coupled ODEs corresponding to the non-dimensional system of heat and mass balance equations to obtain a complete temperature and concentration profile for our reaction system. In order to obtain maximum accuracy, MATLAB's ode15s solver is used with the modified (and more stringent) *RelTol* criteria of 10^{-6}.

Calculations are then performed using Equation (S30), the Seebeck coefficient (S) exhibited by the system, and the chemical potential gradient ($\Delta\mu$) to obtain an output voltage profile with respect to time. This predicted output voltage is then compared with an experimental output voltage. The parameter values that are to be fitted are then varied with the aim of replicating the experimental voltage output.

One point to note is that when fitting or predicting the experimental voltage output using this model, the 'ramping up voltage' as observed in some samples is excluded for the ease of fitting. 'Ramping up voltage' is the minimal voltage output before the actual peak, as seen in some experimental output profiles. One hypothesis for these ramp ups is it being the thermoelectric output from the system while the reaction initiation point heats up one end of the system to the minimum temperature needed for the reaction to initiate. By excluding this portion of the voltage output, we can focus on fitting the main voltage output peak that carries more important data about the reaction wave propagation, device efficiency, and operation.

We performed this fitting analysis for a set of nitrocellulose-SWNT samples showing a wide variety of outputs, such as voltage profiles showing one single polarity peak, multiple single polarity peaks, double polarity peaks, etc. Table 6 contains a list of the 7 parameters that are fitted and how their numerical values can be analyzed to obtain more information about the system.

Table 6: Interpreting from the numerical values for the fitted parameters.

Parameter	***Interpretation***
g_e, ($A_{surface}/V$) or w_{rad}, h_{conv} or w_{conv}	Sample to sample variation in heat losses. This could be representative of the sample contacts or the changes in the surrounding conditions when launching these reaction waves.
S and $\Delta\mu$	Seebeck Coefficient of the TPW system depends not only on the conduit but is also impacted by the presence of the fuel layer atop the thermal conduit

	and thus indicative of the level of contact between the fuel layer and the thermal conduit and hence can vary from device to device. Similar to the Seebeck coefficient, the Chemical Potential Gradient (Coulombs-Volts) strongly depends on how intimate of a contact exists between the thermal conduit and the fuel layer.
k_0, E_a	Arrhenius pre-exponential factor (s^{-1}) is indicative of the nitrocellulose chemical reaction and as such should remain invariant across samples.

References for the Supporting Information

1 WebBook of NIST (National Institute of Standards and Technology) material measurement laboratory.

2 Abrahamson, J. T. *et al.* Excess thermopower and the theory of thermopower waves. *ACS Nano* **7**, 6533–6544 (2013).

3 Betterton, E. A. Environmental fate of sodium azide derived from automobile airbags. *Critical Reviews in Environmental Science and Technology* **33**, 423–458 (2003).

4 Secco, E. A. Thermal decomposition of sodium azide crystals. *Journal of Physics and Chemistry of Solids* **24**, 469–473 (1963).

5 Farhat, H. *et al.* Phonon softening in individual metallic carbon nanotubes due to the Kohn anomaly. *Physical Review Letters* **99**, 145506–145509 (2007).

6 Abrahamson, J. T., Strano, M. S. Analytical solution to coupled chemical reaction and thermally diffusing systems: applicability to self-propagating thermopower waves. *The Journal of Physical Chemistry Letters* **1**, 3514–3519 (2010).

7 Kane, C. *et al.* Temperature-dependent resistivity of single-wall carbon nanotubes. *EPL (Europhysics Letters)* **41**, 683–688 (1998).

8 Abrahamson, J. T. *et al.* Wavefront velocity oscillations of carbon-nanotube-guided thermopower waves: nanoscale alternating current sources. *ACS Nano* **5**, 367–375 (2010).

9 Chen, J. K. & Brill, T. B. Thermal decomposition of energetic materials 50. Kinetics and mechanism of nitrate ester polymers at high heating rates by SMATCH/FTIR spectroscopy. *Combustion and Flame* **85**, 479–488 (1991).

10 Kim, C., Thomas, S. W., Whitesides, G. M. Long-duration transmission of information with infofuses. *Angewandte Chemie International Edition* **49**, 4571–4575 (2010).

11 Hone, J., Batlogg, B., Benes, Z., Johnson, A. T., Fischer, J. E. Quantized phonon spectrum of single-wall carbon nanotubes. *Science* **289**, 1730–1733 (2000).

12 Hone, J., Whitney, M., Zettl, A. Thermal conductivity of single-walled carbon nanotubes. *Synthetic Metals* **103**, 2498–2499 (1999).

13 Thess, A. *et al.* Crystalline ropes of metallic carbon nanotubes. *Science* **273**, 483–487 (1996).

14 Collins, P. G., Avouris, P. Nanotubes for electronics. *Scientific American* **283**, 62–69 (2000).